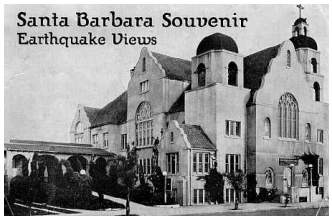

4th IASPEI / IAEE International Symposium:

Effects of Surface Geology on Seismic Motion

August 23–26, 2011 · University of California Santa Barbara

NUMERICAL STUDY OF TOPOGRAPHICAL SITE EFFECTS BY A DISCONTINUOUS FINITE ELEMENT METHOD

Nathalie Glinsky
LRPC/CETE Méditerranée and
INRIA Sophia Antipolis Méditerranée
France

Etienne Bertrand
CETE Méditerranée
Nice
France

ABSTRACT

The examination of the experimental records allows studying local seismicity and teleseismic events in various sites and in many geological configurations. Their processing produces site transfer functions that prove that each site has its own response. Numerical simulation is an interesting tool to understand and try reproducing these phenomena. Thus, we propose to study, using a discontinuous finite element method, the amplification, the concerned frequencies and their distribution along a realistic two-dimensional profile of the Rognes area (France). For this, we examine the seismic response of this profile to series of vertical plane waves whose frequencies vary between 0.2 to 10.0Hz. We also compare the results obtained for several homogeneous and heterogeneous configuration of the medium. The choice of the reference for the site/reference standard spectral ratios is also discussed. Finally, these results are compared to real measurements data proving the ability of this method to deal with such problems.

INTRODUCTION

Many experimental records have been performed during the last 20 years by the CETE Méditerranée Seismic Risk team. This allowed recording local seismicity and teleseismic events in different sites, in France and elsewhere, and in many geological configurations: sedimentary basins, deep alluvial sites, topographic profiles and flat rock sites. Their processing produces site transfer functions that prove that each site has its own response (Bertrand *et al.*, 2011, Duval, 2007). Our objective, in this paper, is to realise numerical simulations of wave propagation on a realistic topography in order to reproduce and understand the observed ground motion amplifications and their variability.

Computational seismology has become a very important topic, thanks to a better understanding of physical phenomena and a constant increase of the computational resources. Thus, it can be now applied to a wide range of applications, from the study of the wave propagation in a topography or in sedimentary basins to more realistic earthquake scenario simulations providing accurate ground motion estimations. Within the last few decades, several numerical methods have been developed. Among all these, we use the discontinuous Galerkin finite element method (Delcourte *et al.,* 2009).

The discontinuous Galerkin method (DG), initially introduced for the solution of neutron transport problems (Reed *et al.,* 1973), has known a renewed interest from the 90's in many applications whose solutions involve hyperbolic problems especially computational electromagnetics. In spite of its success in many domains of application, this method has been only recently applied to seismic wave propagation problems (Käser *et al.,* 2008 and references herein, Delcourte *et al.,* 2009). In comparison with other methods, it has many advantages: 1) it is well adapted to heterogeneous media since it can easily deal with discontinuous coefficients or solutions, 2) the use of simplicial meshes (triangles/tetrahedral), possibly unstructured or locally refined, allows an accurate approximation of the topography, 3) it is naturally adapted to a high order of the unknown field; moreover, the degree of approximation can be increased in the whole domain or very locally, 4) when the discretization in space is coupled to an explicit time integration scheme, the DG method leads to an easily invertible block diagonal mass matrix independently of the form of the local approximation which is a striking difference with classical, continuous finite element formulations. Its main drawback is the number of unknowns, since each mesh

element possesses its own degrees of freedom, which can be readily overcome, especially in three dimensions of space, since the method is easily parallelized.

This paper is organized as follows. In the next section, we present, very briefly, the equations and some characteristics of the numerical method. Then, we detail the studied test case and, finally, the last section presents and analyses the numerical results corresponding to several simplified homogeneous and heterogeneous configurations. These results are also compared to real measurements data.

EQUATIONS AND NUMERICAL METHOD

We consider a two-dimensional isotropic, linearly elastic medium and solve the first-order velocity-stress system in time-domain which writes

$$\begin{cases} \rho \partial_t \vec{v} = \nabla \cdot \sigma, \\ \partial_t \sigma = \lambda (\nabla \cdot \vec{v}) Id + \mu \left(\nabla \vec{v} + (\nabla \vec{v})^T \right), \\ \sigma \vec{n} = \vec{0} \quad on \ free surface \end{cases} \tag{1}$$

where the unknowns are the velocity vector $\vec{v}$ and the stress tensor σ. ρ, λ and μ are respectively the density of the medium and the Lamé coefficients. Id is the identity matrix and ∂_t stands for ∂ / ∂_t. This system is rewritten in matrix form

$$\partial_t \vec{W} + \sum_{\alpha \in \{x,z\}} A_\alpha (\rho, \lambda, \mu) \partial_\alpha \vec{W} = 0 \tag{2}$$

where $\vec{W} = (v_x, v_z, \sigma_{xx}, \sigma_{zz}, \sigma_{xz})$ and the matrices A_α are extra-diagonal by blocks. A detailed description of the method and the expression of the matrices can be found in Delcourte *et al*. (2009), our objective being here to present the method very roughly. The physical domain is discretized using a finite element type mesh in triangles T_i (for $i = 1, N_T$). The interpolation is based on Lagrange polynomials of degree m (m=1, 2, 3 or 4) and for each triangle, we define N_D interpolation points and N_D basis functions φ_k (N_D depends on m). Thus, each component w of the vector $\vec{W}$ is approximated on T_i by $w(x,z,t) = \sum_{j=1}^{N_D} w_j(t) \varphi_j(x,z)$, the terms $w_j(t)$ being the degrees of freedom on T_i, i.e. the unknowns of the problem. (ρ, λ, μ) are assumed to be constant over each element. Equation 2 is multiplied by a basis function and integrated on T_i which leads, after an integration by part to

$$\int_{T_i} \partial_t \vec{W} \varphi_k \, dx\, dz - \sum_{\alpha \in \{x,z\}} A_\alpha^{T_i} . \int_{T_i} \partial_\alpha \varphi_k \vec{W} \, dx\, dz + A_n^{T_i} . \int_{\partial T_i} \varphi_k \vec{W} \, ds = 0 \tag{3}$$

where $A_n^{T_i} = \sum_{\alpha \in \{x,z\}} A_\alpha^{T_i} . n_\alpha$ and $\vec{n} = (n_x, n_z)$ is the outwards unit normal vector to ∂T_i. Note that, compared to the classical finite element method, the volume matrices are local (defined only on T_i) and we obtain additional matrices on the boundary of the element (last term of equation 3) which correspond to the numerical fluxes. The local mass matrices are $N_D \times N_D$ and easily invertible. For the flux integral on the boundary of the element, we split this boundary as the sum of three types of edges : 1) internal edges between two triangles on which a centered flux is introduced, 2) edges on the topography on which a free surface condition is applied and 3) edges on the boundary of the domain where an upwind scheme allows setting the values of the incident plane wave. For the time integration, we apply a second order leap-frog scheme.

DESCRIPTION OF THE TEST CASE

The Provence earthquake (estimated magnitude 6., Chardon and Bellier (2003)), which occurred in 1909 in the south of France, is the most significant French earthquake of the 20th century. It particularly caused severe damage in the small village of Rognes, built on the Foussa hill, probably due to site effects. To highlight this, the CETE Méditerranée Seismik Risk team conducted a field operation, between 2007 and 2009, achieving continuous recordings on nine selected sites (see Fig. 1 for some of them). This campaign allowed recording and analyzing more than 70 earthquakes (10 local events and 60 teleseismic events). Three processings have been conducted from these data: H/V ratio on ambient vibrations, H/V ratio on earthquakes and site/reference standard spectral ratios (SSR) on earthquakes (Duval *et al.,* 2009).

In order to reproduce numerically the results obtained by Duval *et al.* (2009), using the 2D numerical method described previously, we do a south-north cross-section of the Foussa hill as shown on Fig. 1. From the coordinate system (x positive north and z positive upward), we consider a two dimensional domain where the upper boundary is the topography (as shown on Fig. 2) on which a free surface condition is applied. The numerical domain is large enough to avoid spurious reflections from the three other boundaries. Seven sensors are virtually placed at different positions on the hill surface (as shown on Fig. 2), the station 5 being located very similarly to the "FOUH" site of the real data set. As for real measurements, a reference sensor is added in the flat part of the topography, at about 300m of the hill. The numerical domain is 10km wide and 4km deep. The mesh is composed of 512 000 triangles whose smallest edge is 12.5m.

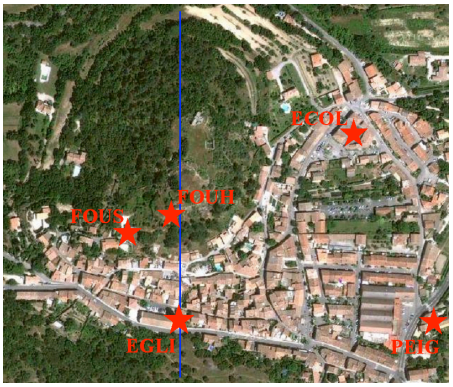

Fig. 1. Aerial photography of the studied zone. The blue line (approximatively 1000m length) corresponds to the south-north profile used in the modelling.

In order to test the sensitivity of the model to its geometry and to the input parameters, we consider several types of configurations. First, we work on a homogeneous case and we study three different types of media of increasing velocities, referred as M1, M2 and M3 and whose properties are listed in the table 1. In a second step, since no data about the hill geology are available, the medium is supposed heterogeneous and constructed by introducing some parts of low velocity medium M1 in the computational domain containing the medium M2. Two cases are studied. In the first one, a 25m thick low velocity layer is introduced just under the free surface, as symbolised by the red line in Fig. 2 (left picture). Under this line, the medium is homogeneous and its characteristics are those of the medium M2. The second heterogeneous configuration supposes that the entire hill is constituted by the medium M1, that is the area between the surface and the red line, as described in the right picture of the Fig. 2. As previously, under this line, the

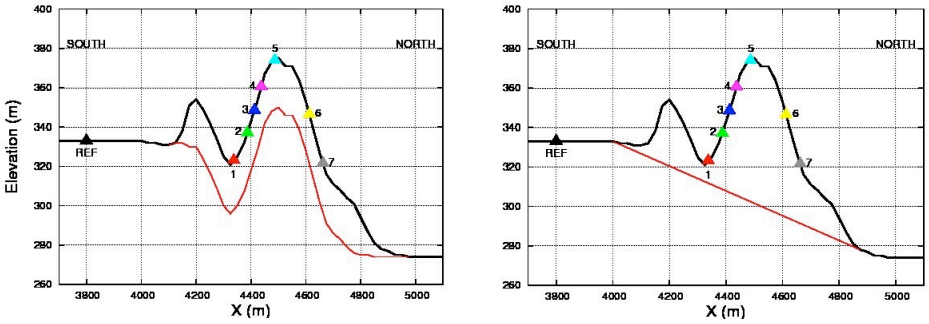

Fig. 2. South-north 2D profile of the Rognes area and sensors location. The two figures describe the different heterogeneous configurations: low velocity layer (left) and low velocity hill (right). In both cases, low velocity medium between surface and red line.

medium is homogeneous and has the characteristics of the medium M2. At last, the influence of the contrast between the two media is studied by considering the two previous models but replacing the medium M2 by the medium M3. In summary, we consider four heterogeneous configurations: the low velocity layer (medium M2/layer M1 and medium M3/layer M1) and the low velocity hill (medium M2/hill M1 and medium M3/hill M1).

Table 1. Characteristics of the three different media used for the homogeneous and heterogeneous cases

	ρ (kg/m²)	P-wave velocity (m/s)	S-wave velocity (m/s)	Poisson ratio
M1	1500	935	500	0.3
M2	2000	1870	1000	0.3
M3	2100	3000	1604	0.3

For a given medium (homogeneous or heterogeneous), we proceed to the propagation of series of vertical S-plane waves by solving equation 1. In order to cover the whole frequency range that we are interested in, the incident waves are Ricker wavelets of central frequency varying from 0.2Hz to 10.0Hz (21 simulations). For each simulation (i.e. for an incident wave of central frequency fc) and at each station, we obtain the velocity time history of both velocity components. Then, for a given central frequency, we apply the following procedure: 1) we compute the spectrum of the horizontal velocity for each station as well as the reference one and 2) we calculate the amplification ratios (station over reference) in an interval centred on fc. Then, for a given station, we construct the seismic response curve, for frequencies between 0.02Hz and 20.0Hz, by gathering the common parts provided by the 21 simulations. In practice, for a given medium configuration, the amplification curves obtained with the different Ricker inputs are identical for a wide interval containing their fc; then, it is not necessary to proceed to 21 simulations to cover the frequency range of interest.

NUMERICAL RESULTS

Choice of the reference solution

For all types of media configurations, solutions have been obtained at the surface stations but also at the reference station, placed in an homogeneous and flat part of the computational domain, far from the topography (see Fig. 2). Unlike real measurements, the incident wave is available. Thus, in the flat case, its value in surface is known and it is interesting to compare the SSR curves obtained when the reference solution is the exact solution of the flat case or the solution obtained at the reference station.

For this, we study more precisely the solutions obtained at the station 5, located at the top of the hill, for the homogeneous case (medium M2), the low velocity layer (medium M2/layer M1) and the low velocity hill (medium M2/hill M1) in the particular case of an incident wavelet of central frequency fc=5.0Hz. We plot, on Fig. 3, the values of the horizontal velocity at the station 5 and at the reference station. We also superimpose the flat case exact solution referred to reference solution afterwards (red curve). From the observation of the figure, we notice: i) at station 5 (upper pictures), an amplification due to the topography in the homogeneous case and a greater increase in amplitude for both heterogeneous configurations; the multiple reflections inside the low velocity area are also visible, especially in the hill case, for which the signal duration is longer and ii) the comparison between the time histories at the reference station and the reference solution (lower pictures) indicates that, if the curves are identical until t=0.8s, they are clearly different after because of surface waves generated at the topographical area. These differences are even larger in the heterogeneous cases.

We compare, in Fig. 4, the spectra corresponding to the time profiles plotted in Fig. 3; note that no smoothing has been applied to the results of this paper. If the amplification at station 5 is obvious, we unfortunately note substantial differences between the spectra of the reference solution and the reference station, proving that this station is influenced by the topography and low velocities areas of the computational domain even if it has been placed far from the hill.

Finally, we present, in Fig. 5, the seismic response at station 5, in the homogeneous and heterogeneous cases, obtained by collecting the results corresponding to incident waves of central frequencies between 0.2 and 10.0Hz. Amplification ratios have been calculated by respect to the reference station (black curves) and by respect to the reference solution (red curves). The two solutions are relatively

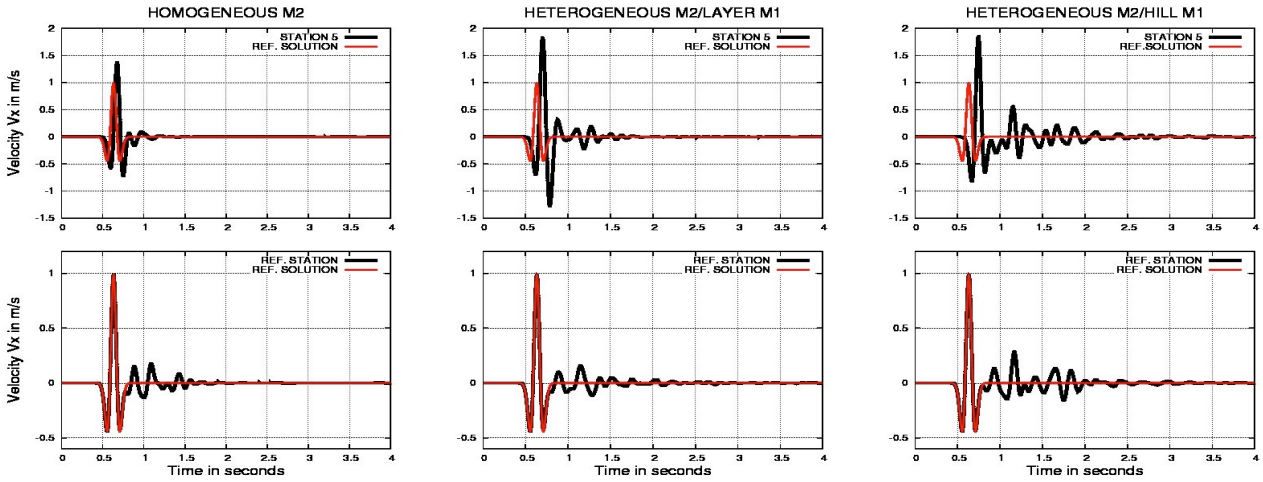

Fig. 3. Horizontal velocity (m/s) as a function of time (s) at station 5 (upper graph) and at the reference station (lower graph). Incident wavelet of central frequency fc=5.0Hz. Homogeneous medium (M1, left column) and heterogeneous media (medium M2/layer M1, central column and medium M2/hill M1, right column). The red profile represents the reference solution.

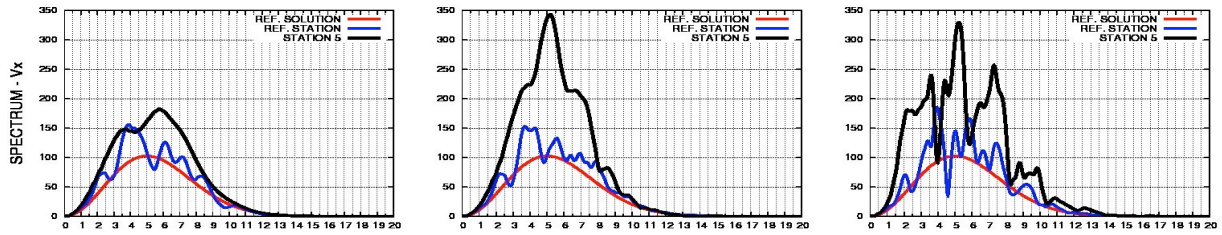

Fig. 4. Spectra of the horizontal velocity of the reference solution (red lines), the reference station (blue lines) and station 5 (black lines) for fc=5.0Hz. Left figure corresponds to the homogeneous medium M2, heterogeneous layer (medium M2/layer M1) at the center and heterogeneous hill (medium M2/hill M1, right figure).

different and, on the results corresponding to the reference station, appear amplifications at additional frequencies, compared to ratios obtained by respect to the reference solution. This is due to the division of spectral values from non smooth curves (black curve on blue curve of Fig. 4). This is particularly visible in the last heterogeneous case (right figure) for which a totally artificial amplification is obtained at 4.5Hz. These results could be probably improved by positioning the reference station at a greater distance from the hill,

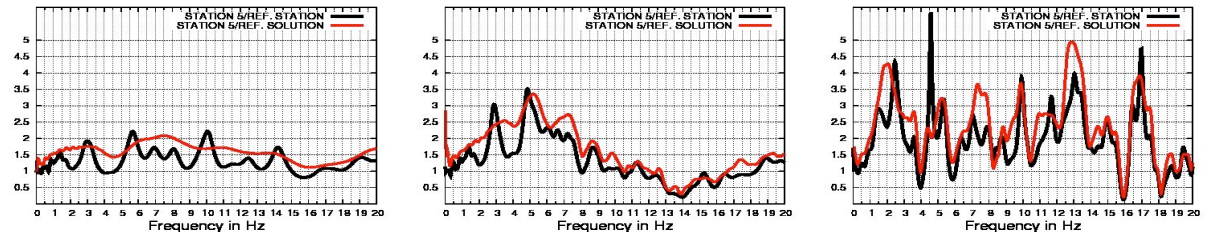

Fig. 5.Seismic response of the homogeneous and heterogeneous profiles to vertical S-plane waves for frequencies between 0.02 and 20.0Hz. Solutions obtained at station 5 by respect to the reference station (black curves) and the reference solution (red lines). Left figure corresponds to the homogeneous medium M2, heterogeneous layer (medium M2/layer M1) at the center and heterogeneous hill (medium M2/hill M1, right figure).

extending uselessly the computational domain (and the CPU time). So, in the rest of the study, spectral ratios are calculated by respect to the reference solution only.

Homogeneous medium

Firstly, we consider the case of a homogeneous medium and study the three different media described in table 1. Following the procedure previously detailed, we plot in Fig. 6 the amplification calculated in these homogeneous cases. Each figure corresponds to a

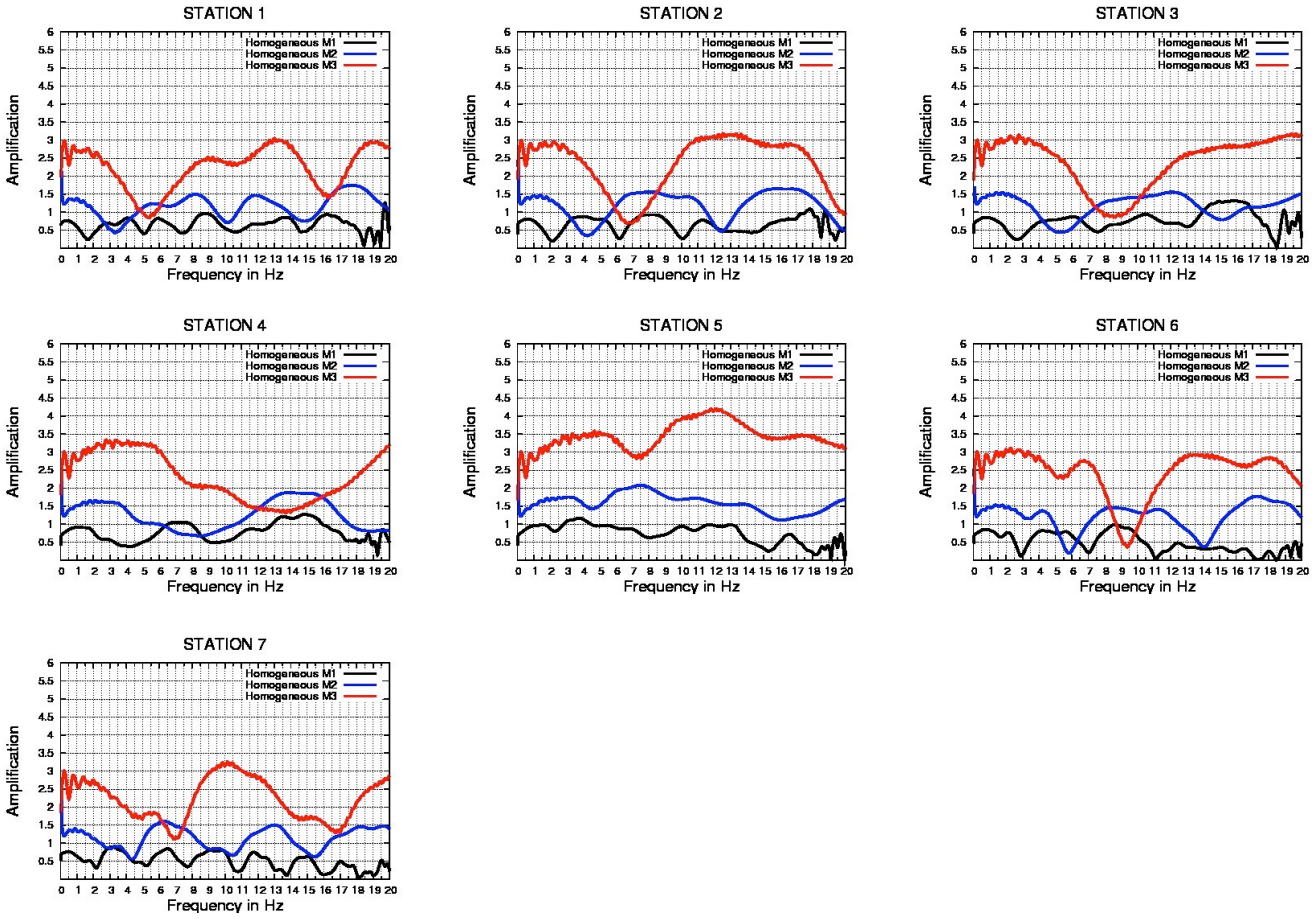

Fig. 6.Seismic response of the homogeneous profiles to vertical S-plane waves for frequencies between 0.02 and 20.0Hz. Each picture corresponds to a station, black curves for medium M1, blue curves for medium M2 and red curves for medium M3.

station and the red, blue and black curves are the solutions corresponding to the media M1, M2 and M3 respectively. From the review of this series of results and if we suppose that amplification corresponds to ratios greater or equal to 1.5, we notice that: i) the amplification is strongly relied to the medium velocity. No amplification is observed for the lower velocity medium (M1, black curves) whereas a moderate amplification is obtained for medium M2 (blue curves) since ratios reach values between 1.5 and 2.0. The most important amplifications correspond to the fastest velocity medium M3 (red curves) for which maximum ratios are between 3.0 and 4.0, ii) the most important amplification is obtained at the top of the hill (station 5) and iii) the amplification frequencies depend on the medium velocity, a higher velocity medium leading to higher values of the response frequency. For instance at station 5, amplification occurs at 2.5Hz and 7.0Hz for medium M2 and at 5.0Hz and 12.0Hz for medium M3.

Heterogeneous medium – Influence of the model in depth-geometry

In a second step, the medium is supposed heterogeneous and we study the two configurations described in Fig. 2. In order to examine the influence of the geometry of the low velocity zone on the results, we suppose that the computational domain is made of medium M2 and the properties of the low velocity zone (layer or hill, see Fig. 2) are those of the medium M1. We follow the same procedure

as in the homogeneous case and present in Fig. 7 the amplification ratios at the stations for the homogeneous case and the two heterogeneous configurations. As previously, each figure corresponds to a station, the black curves to the homogeneous case (medium M2), the blue lines to the heterogeneous layer (medium M2/layer M1) and the red curves to the heterogeneous hill (medium M2/hill M1). From the observation of the results, we remark that: i) the introduction of surface low velocity zones increases significantly the amplification values. In the homogeneous case, the maximum ratio is 2.0 at station 5 and about 1.5 at other stations. In the heterogeneous layer case, ratios reach 2.0 at stations 2 and 3, are about 2.25 for stations 1, 4, 6 and 7 and greater than 3.0 at the top of the hill (station 5). The most important amplifications are obtained for the heterogeneous hill case since ratios are greater than 4.0, for all stations, ii) in the homogeneous case, amplification is mainly obtained at the top of the hill. In the heterogeneous cases, amplification also occurs at other stations, especially for the heterogeneous hill configuration, iii) the amplification frequencies are

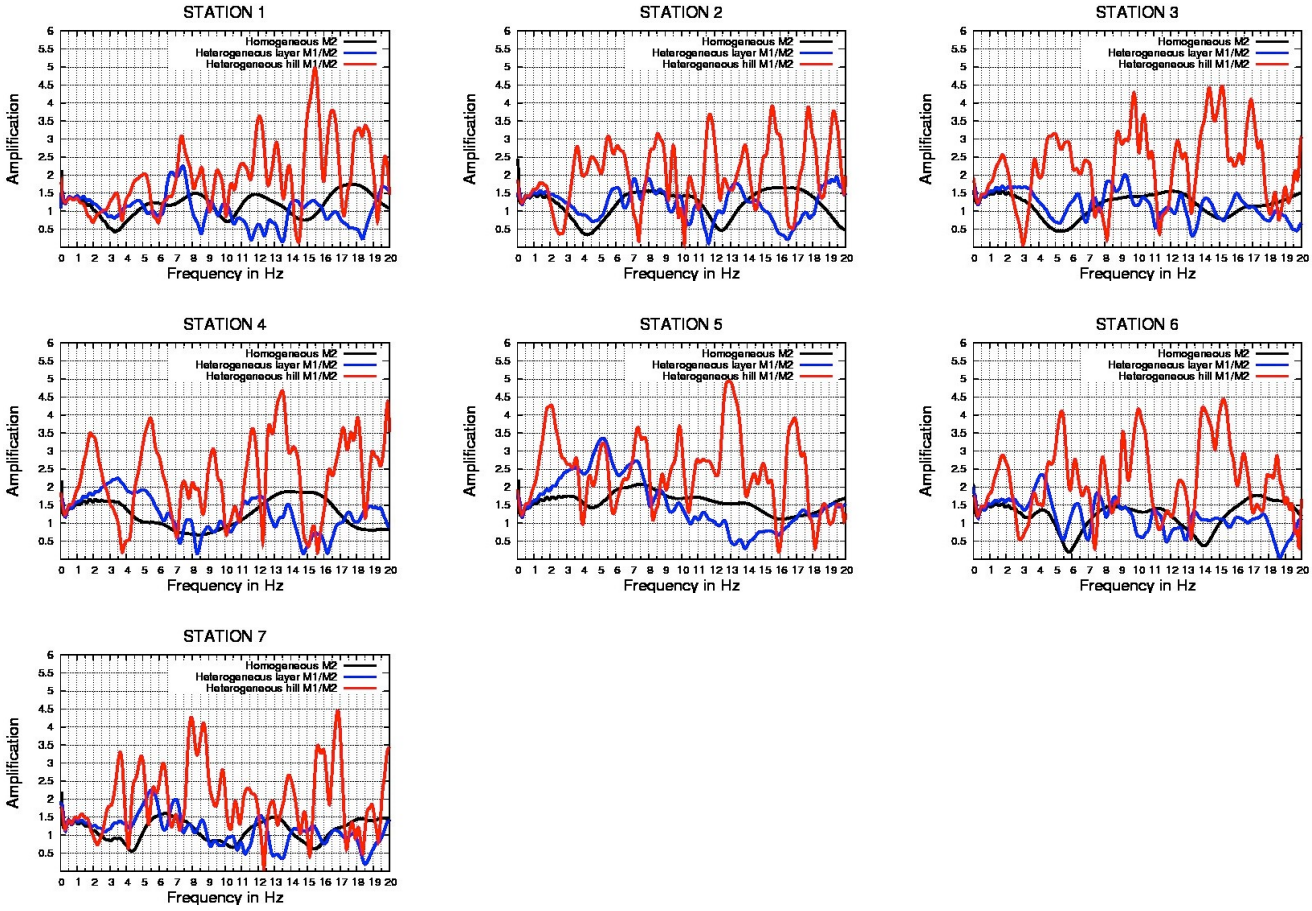

Fig. 7.Seismic response of the homogeneous and heterogeneous profiles to vertical S-plane waves for frequencies between 0.02 and 20.0Hz. Each picture corresponds to a station, black curves for homogeneous case (medium M2), blue curves for heterogeneous layer (medium M2/layer M1) and red curves for heterogeneous hill (medium M2/hill M1).

strongly dependent on the heterogeneous configuration. In the heterogeneous layer case, amplifications are obtained for frequencies between 3.5Hz and 5.0Hz whereas, for the heterogeneous hill configuration, these frequencies are reduced and equal to 2.0Hz, at stations 3, 4, 5 and 6. These results prove that the solutions are very dependent of the model in-depth geometry.

Heterogeneous medium – Influence of the model velocity contrast

We have also studied the influence of the model velocity contrast, in the heterogeneous case. For this, we consider the two configurations already studied in the previous section and introduce a greater contrast between the two media by replacing the medium M2 by the medium M3. Following the same treatment of the results, we present, on Fig. 8, the seismic response at three particular stations (4, 5 and 7) and we compare, for both the layer case (first line of pictures) and the hill configuration (second line of pictures), the results obtained for the two types of medium contrast (M2/M1, black curves and M3/M1, red curves). Note that different vertical

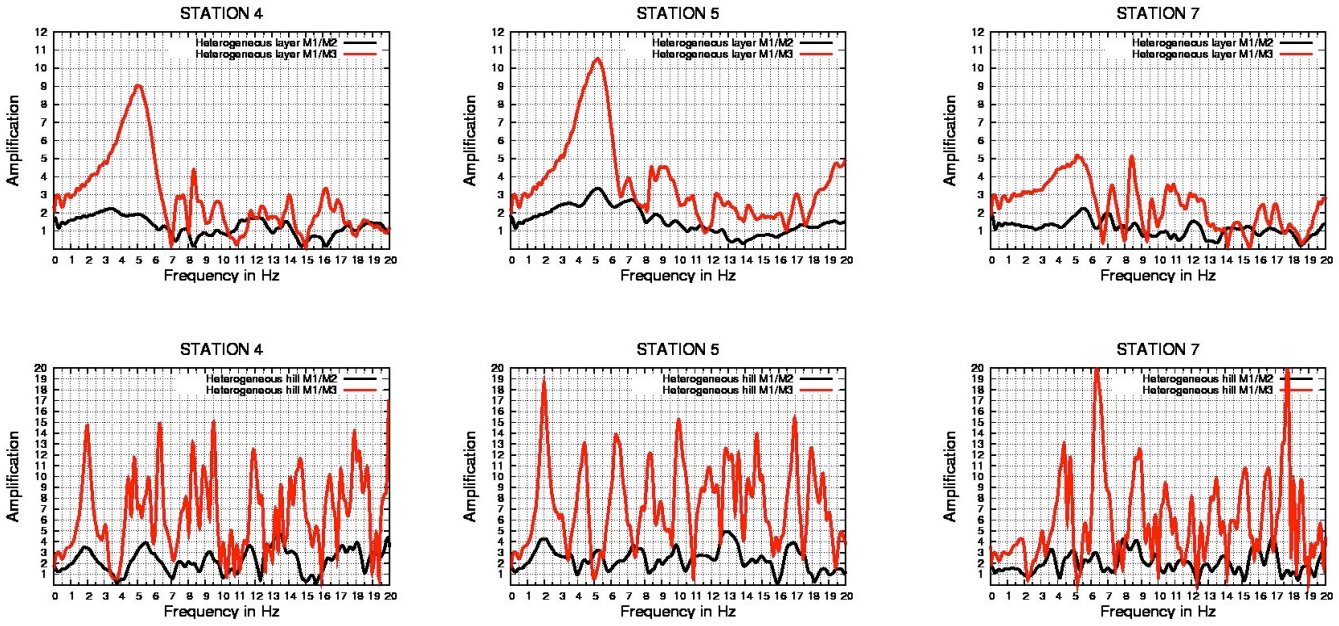

Fig. 8.Seismic response of the heterogeneous profiles to vertical S-plane waves for frequencies between 0.02 and 20.0Hz at stations 4, 5 and 7. The upper pictures represent the layer case (medium M2/layer M, black curves and medium M3/layer M1, red curves) and the lower pictures the hill case (medium M2/hill M1, black curves and medium M3/hill M1, red curves).

scales have been used for the two series of figures. When examining these results, we notice that: i) for both configurations (layer or hill), the use of high contrast media results in a noticeable increase of the amplification values, which are multiplied approximatively by a factor 4.0, ii) the value of the fundamental frequency is unchanged but the values corresponding to higher modes are reduced in the case of higher contrast media.

Comparison with experimental data

For a comparison with the real measurements data, we present, in Fig. 9 (top picture), the seismic response derived from near earthquakes recordings at three sites presented on Fig. 1 (Duval *et al.,* 2009). The stations of our two-dimensional profile have been placed along the topography in order to be compared to real sites ones: station 4 to FOUS, station 5 to FOUH (at the top of the hill) and station 7 to ECOL (at low altitude). We also reproduce the seismic response obtained by our simulations at these stations, in the case of the heterogeneous layer and the heterogeneous hill. In both cases, the left column represents the weak interface model (M2/M1) and the right column the strong interface model (M3/M1). Note that the same colour code has been chosen for a better comparison between the real sites data and the numerical solutions at the corresponding stations.

From the comparison between measurements and numerical solutions, we notice that: i) the results obtained using a heterogeneous layer are very different from the real data. If maximum and minimum amplification values are obtained at station 4 (turquoise curve) and station 7 (grey curve) as for measurements, the frequencies corresponding to these extrema are too high (5.0Hz for simulations and 2.0Hz for measurements), ii) the numerical solutions corresponding to the heterogeneous hill are very close to the real data. The amplification measured at FOUH is about 10.0 which is somewhere between the values obtained for the two types of media contrast (4.0 for media M2/M1 and 16.0 for M3/M1). The highest amplification is obtained at a frequency equal to 2.0Hz for stations 4 and 5 of our model as for stations FOUH and FOUS. However, the maximum for station ECOL corresponds to a higher frequency value equal to 5.0Hz which is slightly different to the computed frequency at station 7 (3.5Hz). Note that we have supposed that the medium is linearly elastic; this can explain the differences at high frequencies. Considering the fact that the numerical simulations are obtained on a simplified two-dimensional heterogeneous model, for which no data concerning the in-depth geology is available, these results are very encouraging.

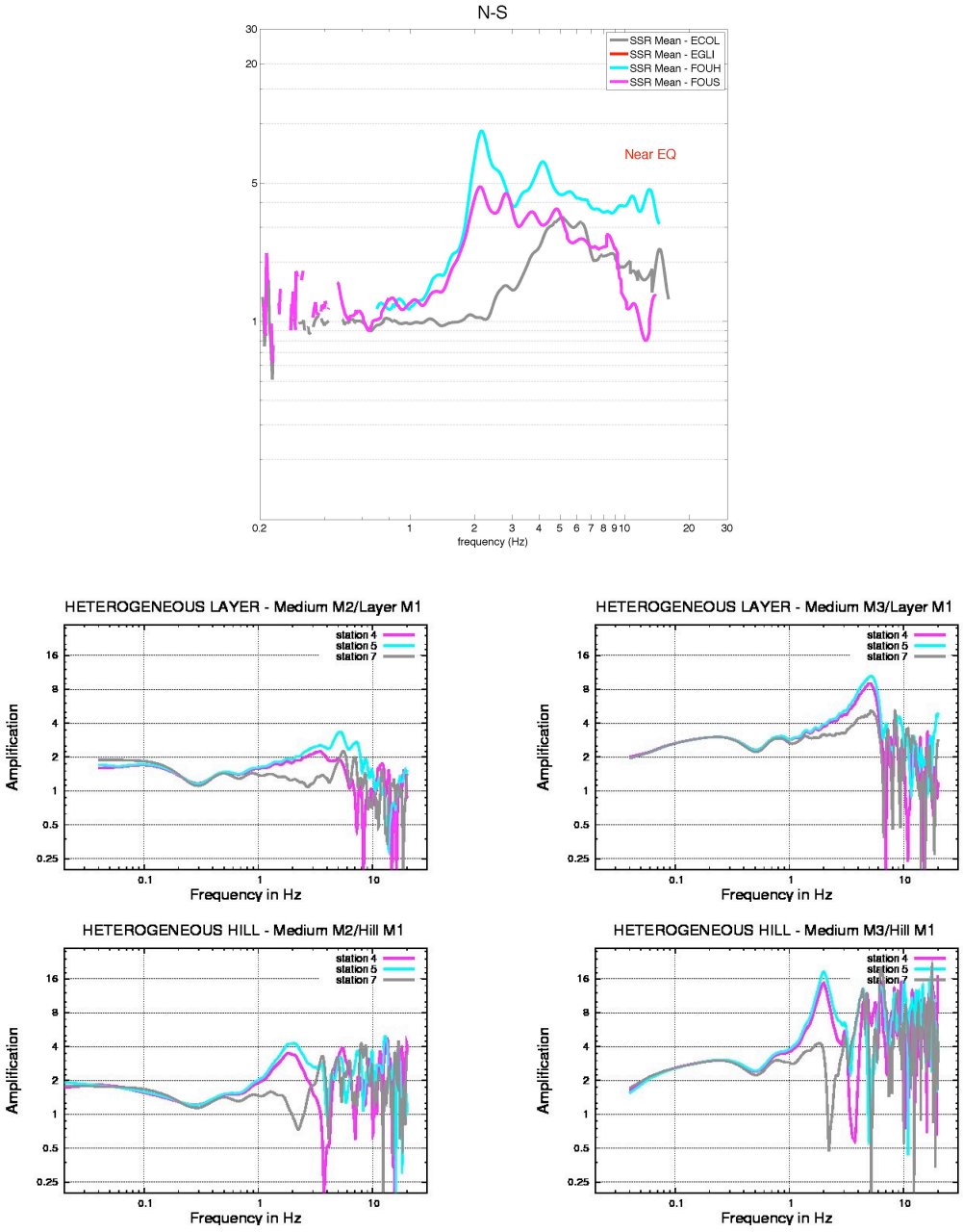

Fig. 9.Seismic response at three stations from real measurements for near earthquakes (uppermost figure) and from numerical simulations. The upper line of numerical results represents the heterogeneous layer case and, the bottom line, the heterogeneous hill case.

CONCLUSION

We present a study of topographical effects using a discontinuous finite element method. This method allows an accurate approximation of the topography via the use of triangular meshes and an easy inclusion of heterogeneities. We have considered a two-dimensional simplified model of the Rognes area and several homogeneous and heterogeneous configuration in order to study the spectral response of this profile to series of vertical S-waves of various central frequencies. We have tested the sensitivity of the model

to some parameters such as the medium characteristics for homogeneous configurations, the medium in-depth geometry and the contrast between the media in the heterogeneous cases. This study proves that the results are very dependent on the model configuration, especially in the heterogeneous case. These numerical simulations have been compared to real measurements data and the results obtained supposing a low velocity hill are very comparable to the real measurements data. This proves the ability of the method to deal with such problems and the need to describe as accurately as possible for accurate numerical solutions.

Two directions of improvement are currently under consideration, the extension of such a study to the three-dimensional case and a more realistic topography of the Rognes area and better results at high frequencies by taking into account material attenuation in the system of equations.

REFERENCES

Bertrand, E., A.-M. Duval, J. Régnier, R. M .Azzara, F. Bergamaschi, P. Bordoni, F. Cara, G. Cultrera, G. Di Giulio, G. Milana and J. Salichon J. [2011], "Site effect of the Roio Basin, L'Aquila", Bull. Earthq. Eng, Vol. 9,No.3, pp. 809-823. Produit LCPC OP11R065/2010/ERA6/21.

Chardon D. and O. Bellier [2003], "Geological boundary conditions of the 1909 Lambesc (Provence, France) earthquake: structure and evolution of the Trévaresse ridge anticline", Bulletin de la Société Géologique de France, Vol. 174, No.5, pp. 497-510.

Delcourte S., L. Fezoui L. and N. Glinsky-Olivier N. [2009], **"** A high-order discontinuous Galerkin method for the seismic wave equation **"**, ESAIM:Proceedings, Vol. 27, pp. 70-89.

Duval A.-M. [2007], « Des effets de site aux scénarios de crise sismique : méthodes et applications », Habilitation à Diriger des Recherches, Université des Sciences et Technologies de Lille.

Duval A.-M., E. Bertrand, J. Régnier, N. Glinsky, P. Langlaude, M. Pernoud, S. Vidal, J. Gance, E. Grosso and J.-F. Semblat [2009], "Experimental and numerical approaches of topographic site effect claimed to be responsible for 1909 Provence earthquake damage distribution", American Geophysical Union, Fall Meeting*,* San Francisco.

Glinsky N., E. Bertrand, A.-M. Duval, J. Régnier and S. Lanteri [2010], **"** Numerical study of site effects by a discontinuous Galerkin finite element method **"**, Proceedings of 14th European Conference on Earthquake Engineering 14ECEE 2010, Ohrid, Rep. of Macedonia, august 30-september 03.

Käser M., V. Hermann and J. de la Puente [2008], **"** Quantitative accuracy analysis of the discontinuous Galerkin method for seismic wave propagation **"**, Geophys. J. Int., Vol. 173, No.3, 2008, pp. 990-999.

Reed W. and T. Hill T. [1973], **"**Triangular mesh method for neutron transport equation", Tech. Rep. LA-UR-73-479, Los Alamos Scientific Laboratory.